REVISTA INTERDISCIPLINAR DE PESQUISA EM ENGENHARIA

CILAMCE 2016

XXXVII IBERIAN LATIN AMERICAN CONGRESS ON COMPUTATIONAL METHODS IN ENGINEERING
BRASÍLIA - DF - BRAZIL

FLOW OF ELLIPTICAL PARTICLE SUSPENSIONS THROUGH A CONVERGING-DIVERGING CHANNEL

Ivan Rosa de Siqueira

Rodrigo Bento Rebouças

ivan@lmmp.mec.puc-rio.br

rodrigobento@lmmp.mec.puc-rio.br

Márcio da Silveira Carvalho

msc@puc-rio.br

Pontifícia Universidade Católica do Rio de Janeiro

Laboratory of Microhydrodynamics and Flow in Porous Media - LMMP, Department of Mechanical Engineering, Pontifícia Universidade Católica do Rio de Janeiro, Rio de Janeiro-RJ 22451-900, Brazil

Abstract. *This work analyzes the flow of elliptical particle suspensions through a converging-diverging channel. The model considers rigid elliptical particles dispersed in a Newtonian liquid, and the suspension viscosity is given by a function of the local particle concentration and particle axis aspect ratio. Shear-induced particle migration phenomena is described by the well-known Diffusive Flux Model, and the average particle orientation is given by the principal direction of a particle conformation tensor. The conformation evolution in the flow and the constitutive equation for the resulting complex liquid are adapted from classical models used to describe the behavior of suspensions of spheroids, cylinders and fibers and polymeric solutions of rod-like molecules that are almost or completely rigid. The resulting set of fully coupled, non-linear equations is solved using a slightly variation of the DEVSS-TG/SUPG Finite Element Method. The results show the local particle concentration and average particle orientation in the flow domain, highlighting the behavior of the suspension microstructure near shear-dominated and extensional-dominated regions.*

Keywords: *Elliptical particle suspensions, Particle migration, Particle alignment, Finite Element Method*

1 INTRODUCTION

A suspension is a heterogeneous two-phase system in which solid particles are dispersed in a liquid medium. In most of the applications, however, the small size of the suspended particles and its quantity dispersed in the basis fluid allow the mixture to be treated as an equivalent continuous medium, whose average mechanical behavior is intrinsically related to the dynamics in the scale of the particles. Typically, suspensions show non-Newtonian behavior, mainly at high concentrations. Indeed, even though the continuous phase is composed by simple liquids, such as water or organic solvents, for example, the physical phenomena that occur in the microscopic scale of the material are very complex, such that the resulting complex fluid shows non-linear effects in many cases (Larson, 1988, 1999; Trados, 2011, 2012). The importance of studying the mechanics and rheology of suspensions is supported by the wide range and scope of its applications. Fundamental understanding of the complex behavior of these materials are important in many sectors of different industries, such as oil and petroleum (Schramm, 1996), coating (Kistler & Schweizer, 1997), and pharmaceutical and comestic (Kulshreshtha et al., 2010).

Since the landmark works of Einstein (1911) and Jeffery (1922) on the viscosity of dilute suspensions of spherical and ellipsoidal particles, much progress has been achieved in this sense. Notwithstanding, the situation for concentrated suspensions is very difficult to analyze. At very high volume fractions in which the particles are near jamming, there is actually no theoretical nor experimental consensus on the concentration dependence of the viscosity (Shewan & Stokes, 2015). Many theoretical models based on effective-medium theories (Krieger & Dougherty, 1959; Krieger 1972) and semi-empirical models based on experimental results (Brady, 1993; Bicerano et al., 1999) have been proposed in order to extend a quantitative description of the suspension viscosity. At large, they tend to recover Einstein's classical result at very low concentrations and diverge at the approach of a maximum packing fraction, which depends on particle shape and arrangement. Recently, Santamaría-Holek & Mendoza (2009, 2010) have developed a continuum-medium description for the viscosity-concentration relation for suspensions of particles with different shapes, including spheres, ellipsoids, cylinders and dumbbells, as long as they are not too elongated. Their model gives excellent quantitative results when compared to experimental data at the whole concentration range for different particle shapes, even at concentrated regimes.

Another complex phenomena that may occur in the flow of concentrated suspensions is related to particle migration across the streamlines in non-homogeneous shear flows, which was first observed by Karnis et al. (1966) and Gadala-Maria & Acrivos (1980). Briefly, their experimental results on pressure-driven flows through tubes and cylindrical Couette flows showed that the suspended particles assume a non-uniform configuration in non-homogeneous shear flows, migrating from high to low shear rate regions. However, the first explicit explanation of the possibility of a cross-stream flux of particles in concentrated suspensions is due to Leighton & Acrivos (1987). From simple scaling arguments, they proposed a general expression for the diffusive flux of particles in unidirectional shear flows. Their hypothesis was that particle migration arises from gradients in shear rate and viscosity, and was confirmed by Nuclear Magnetic Resonance (or NMR) images obtained from cylindrical Couette flows and pressure-driven flows through tubes (Abbott et al, 1991; Altobelli & Givler, 1991; Graham & Altobelli, 1991; Sinton & Chow, 1991). Subsequently, Phillips et al. (1992) extended the latter flux expression

and developed a convection-diffusion equation that describes the evolution of particle concentration profile, establishing the now well-known Diffusive Flux Model (thereafter DFM). Their numerical results from a Finite Difference Method algorithm were compared in good agreement to experimental data also obtained by NMR images of cylindrical Couette and pressure-driven flows. Afterwards, the predictions of the model were confirmed once again for different flows by other researchers using distinct experimental techniques (Chow et al., 1994; Hampton et al., 1997; Han et al., 1999; Koh et al., 1994; Lyon & Leal, 1998; Subia et al., 1998).

On the other hand, when the suspended particles are not spherical, beyond the particle concentration distribution, it is also necessary to predict how the particles are aligned in the flow domain. Recent works of Oumer & Mamat (2013) and Trebbin et al. (2013) have shown that the alignment of suspended long fibers essentially depends on the external flow applied. From their experimental results in converging-diverging flows through tubes, they determined that the particles tend to align with respect to the flow direction in converging flows, as occurs near the entrance of the contraction (i.e. uniaxial extensional zones), and perpendicular to the flow direction in diverging flows, as occurs at the end of the contraction (i.e. biaxial extensional zones). Within this context, this work focuses on the converging-diverging channel flow of a suspension of slightly elliptical particles, and investigate the particle concentration and average particle alignment in the domain, which contains both shear-dominated and extensional-dominated regions. We present a fully coupled, non-linear model accounting for both particle migration and particle orientation in the flow. The governing equations are numerically solved using a variation of the DEVSS-TG/SUPG Finite Element Method. The paper is organized as follows. In §2, we present the complete mathematical formulation of the problem, including details on the calculation of the particle conformation tensor used to measure the average particle orientation in the flow and the constitutive relation used to describe an additional conformation stress depending on particle concentration and particle orientation. Then, §3 is devoted to describe the aspects of the numerical methodology employed. Finally, in §4, we present and discuss extensively the results obtained for both local particle concentration and particle alignment.

2 MATHEMATICAL FORMULATION

Because of typical scales involved in the problem, the suspension of particles can be treated as continuum medium in the converging-diverging channel. Therefore, the flow of the resulting complex liquid is described by incompressible mass conservation and Cauchy's equation of motion, which require that

$$\nabla \cdot \boldsymbol{u} = 0 \tag{1}$$

and

$$\rho \left(\frac{\partial \boldsymbol{u}}{\partial t} + \boldsymbol{u} \cdot \nabla \boldsymbol{u} \right) = \nabla \cdot \boldsymbol{\Sigma} + \rho \boldsymbol{g}, \tag{2}$$

where $\boldsymbol{u}$ is the velocity vector, ρ is the suspension density, $\boldsymbol{\Sigma}$ is the suspension stress tensor and $\boldsymbol{g}$ is a body force per unit mass. The stress tensor is split as $\boldsymbol{\Sigma} = -p\boldsymbol{I} + \boldsymbol{\tau} + \boldsymbol{\sigma}$, where p is the pressure field, which is constitutively indeterminate, $\boldsymbol{I}$ is the identity tensor, $\boldsymbol{\tau}$ is the viscous stress, and $\boldsymbol{\sigma}$ is an additional conformation stress that depends on the local particle concentration and average particle orientation in the flow.

The viscous stress obeys Newton's law of viscosity with a concentration-dependent viscosity, i.e. $\boldsymbol{\tau} = \eta(\phi)(\nabla \boldsymbol{u} + \nabla \boldsymbol{u}^T)$, where η is the suspension viscosity, ϕ is the local particle concentration and the superscript T denotes the transpose operation. Considering differential-effective medium arguments, the suspension viscosity is calculated as (Santamaría-Holek & Mendoza, 2010)

$$\eta = \eta_0 \left[1 - \left(\frac{\phi}{1 - c\phi}\right)\right]^{-[\eta]}. \tag{3}$$

In Eq. (3), $\eta = \eta(\phi)$ is the suspension viscosity, η_0 is the viscosity of the Newtonian solvent liquid and $[\eta]$ is the so-called intrinsic viscosity. In addition, $c = (1-\phi_c)/\phi_c$ is a crowding factor that guarantees that the particles cannot occupy all the volume of the sample due to geometric restrictions, where ϕ_c is the critical concentration of particles at which the suspension loses its fluidity. In the case of elliptical particles, $[\eta]$ and ϕ_c depend on the particle axis aspect ratio p, defined as the ratio between the polar and equatorial radii of a particle, i.e. $p = b/a$. The values of these parameters can be found in Landau et al. (1984) and Donev et al. (2004, 2007).

Shear-induced particle migration is described by the Diffusive Flux Model developed by Phillips et al. (1992). The model sets a typical convection-diffusion equation accounting for particle transport in the flow, such that

$$\frac{\partial \phi}{\partial t} + \boldsymbol{u} \cdot \nabla \phi + \nabla \cdot \boldsymbol{N}_\phi = 0, \tag{4}$$

where $\boldsymbol{N}_\phi$ is the total diffusive flux of particles due to different mechanisms. Particle migration arises from three different physical mechanisms, namely: gradients in shear rate, gradients in viscosity, and curvature of the streamlines. The mathematical expressions for each one of these fluxes are (Phillips et al., 1992; Kim et al., 2008)

$$\boldsymbol{N}_c = -K_c a^2 \phi \nabla(\dot{\gamma}\phi), \tag{5}$$

$$\boldsymbol{N}_\eta = -K_\eta a^2 \left(\frac{\dot{\gamma}\phi^2}{\eta}\right) \nabla \eta, \tag{6}$$

and

$$\boldsymbol{N}_\kappa = K_\kappa a^2 \dot{\gamma} \phi^2 \kappa \boldsymbol{n}. \tag{7}$$

In Eqs. (5), (6) and (7), a is a typical particle size (the equatorial radius of an elliptical particle), $\dot{\gamma}$ is the local shear rate, κ is the local curvature radius of a streamline and $\boldsymbol{n}$ is the unit normal vector in the radially outward direction of a curved streamline. The parameters K_c, K_η and K_κ are diffusion-like coefficients of $\mathcal{O}(1)$ that should be found from experimental results. Here, we assume that $K_c = 0.41$, $K_\eta = 0.62$ and $K_\kappa = K_c$ (Phillips et al., 1992; Kim et al., 2008). Finally, note that the total diffusive flux of particles is given by the summation of these three diffusive fluxes, so that $\boldsymbol{N}_\phi = \boldsymbol{N}_c + \boldsymbol{N}_\eta + \boldsymbol{N}_\kappa$ in Eq. (4).

The orientation of the elliptical particles in the flow is given by a particle conformation tensor, which is defined as $\boldsymbol{M} =< \boldsymbol{rr} >$, where $\boldsymbol{r}$ is the end-to-end vector of a particle and $<>$ denotes average over the distribution of orientations. It is worth mentioning that $\boldsymbol{M}$ is a positive definite symmetric tensor, and, at equilibrium, $\boldsymbol{M} = \boldsymbol{I}$. In order to investigate regions of molecular stretching and molecular extension in complex flows of polymer solutions composed by almost rigid molecules dispersed in a Newtonian medium, Pasquali & Scriven (2002, 2004) proposed an equation accounting for the evolution of the conformation dyadic.

Here, we consider an adaptation of this model to describe the conformation of rigid, elliptical particles, so that the evolution of the dimensionless particle conformation in the flow is given by

$$\overset{\nabla}{\boldsymbol{M}} + 2\frac{\boldsymbol{D}:\boldsymbol{M}}{\boldsymbol{I}:\boldsymbol{M}}\boldsymbol{M} + \frac{1}{\lambda}(\boldsymbol{M}-\boldsymbol{I}) = \boldsymbol{0}. \tag{8}$$

where the superscript ∇ denotes the upper-convected time derivative[1] and λ is the particle relaxation time. The two first terms on the right-hand side of Eq. (8) account for a variation on particle conformation because of the velocity field, whereas the last term represents a relaxation process on the conformation dyadic, which is assumed to be linear with the distance from the value at equilibrium. Therefore, the result of particle conformation is dictated by a balance between the velocity field and the rate of relaxation of the suspension microstructure, which acts to restore the particles to its equilibrium configuration. In this sense, let us define the dimensionless time parameter $\tau = \tau_\lambda/\tau_\infty$, where $\tau_\lambda = \lambda$ is a characteristic scale of time of the suspension microstructure and $\tau_\infty = H/V$ is a characteristic scale of time of the convective transport related to the velocity field. By definition, τ measures the ratio between the effects of particle relaxation to the effects of the velocity field in the conformation transport equation. Once the equation of conformation transport has been solved and the conformation dyadic is known, the average particle orientation can be properly obtained using the orthonormal eigenvectors of $\boldsymbol{M}$, i.e. the principal directions of the second moment of the distribution of orientations. Considering that $\boldsymbol{m}$ is the eigenvector related to the largest eigenvalue of $\boldsymbol{M}$, the average particle orientation with respect to the $\hat{\boldsymbol{e}}_1$-direction is calculated as

$$\theta = \tan^{-1}\left(\frac{|\boldsymbol{m}\cdot\hat{\boldsymbol{e}}_2|}{|\boldsymbol{m}\cdot\hat{\boldsymbol{e}}_1|}\right). \tag{9}$$

We emphasize that the transport of conformation in Eq. (8) is a simplified model to describe the evolution of conformation of elongated particle suspensions. For instance, this approach does not explicit consider the effect of the suspension concentration and particle axis aspect ratio on the conformation evolution, but only in a indirect way through the suspension viscosity in momentum equation.

When the suspension is treated as a continuum medium, particle orientation gives rise to an additional anisotropic viscous stress in suspensions of spheroids, cylinders and long fibers (Larson, 1988, 1999). A quadratic closure approximation can be used to write a simple relation to describe the additional stress due to particle orientation in the flow, so that

$$\boldsymbol{\sigma} = f(p)\eta_M(\phi)\boldsymbol{M}\boldsymbol{M}:\boldsymbol{D}, \tag{10}$$

where $\boldsymbol{D} = (\nabla\boldsymbol{u}+\nabla\boldsymbol{u}^T)/2$ is the rate of strain tensor. Here, $f(p) = (p^2-1)/(p^2+1)$ is a scalar function of the particle aspect ratio and $\eta_M(\phi) = \eta(\phi) - \eta_0$ is the viscosity increment because of the presence of the dispersed particles. Note that $f(p) \to 0$ as $p \to 1$, so that $\boldsymbol{\sigma} = \boldsymbol{0}$ when $p = 1$, meaning that there is no particle alignment, and thereby no additional conformation stress when the particles are spherical. In this case, the stress tensor reduces to a Newtonian stress with a local concentration-dependent viscosity, $\boldsymbol{\Sigma} = -p\boldsymbol{I} + 2\eta(\phi)\boldsymbol{D}$. In turn, the term η_M accounts for dependence of the additional stress on the particle concentration. Note that $\eta(\phi) \to \eta_0$ as $\phi \to 0$, so that $\boldsymbol{\sigma} = \boldsymbol{0}$ when $\phi = 0$, and thereby the stress tensor reduces to the Newtonian constitutive relation $\boldsymbol{\Sigma} = -p\boldsymbol{I} + 2\eta_0\boldsymbol{D}$ when there is no particles in the solvent.

[1] By definition, $\overset{\nabla}{\boldsymbol{M}} = \dfrac{\partial \boldsymbol{M}}{\partial t} + \boldsymbol{u}\cdot\nabla\boldsymbol{M} - \nabla\boldsymbol{u}^T\cdot\boldsymbol{M} - \boldsymbol{M}\cdot\nabla\boldsymbol{u}$.

The fully coupled, non-linear model proposed here is used to study the flow through a converging-diverging channel with a contraction ratio of 4:1. The geometry of the problem is presented in Fig. 1. The channel height at the inflow and outflow planes is $2H$. The domain is subdivided into three distinct regions: upstream the contraction, the contraction, and downstream the contraction. Each region has the same size in length, which is equal to $50H$, and the channel total length is $L = 150H$. The flow is assumed to be symmetric with respect to the $x_2 = 0$ plane, such that only the upper half of the channel was considered in the calculations.

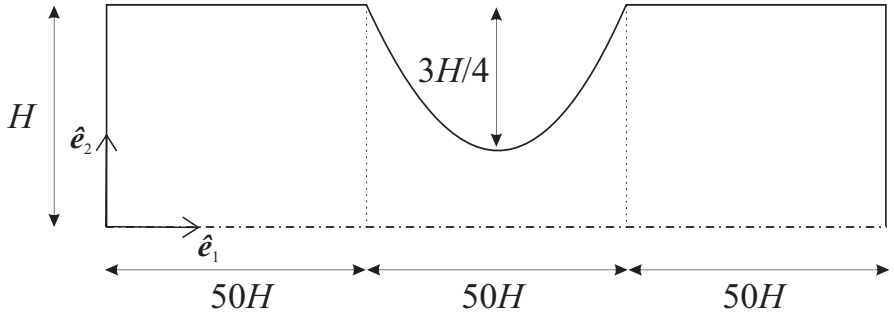

Figure 1: Sketch of the geometry of the problem (not to scale).

The boundary conditions used to solve the transport equations given in Eqs. (1), (2), (4) and (8) are described as follows, where $\boldsymbol{n}$ and $\boldsymbol{t}$ are local unit normal and tangent vectors to the boundaries.

1. **Inflow plane.** We assume a fully developed, parabolic velocity profile $\boldsymbol{u} = u_1(x_2)\hat{\boldsymbol{e}}_1$ with pressure free. Moreover, we considered that the suspension concentration is uniform and equal to the bulk concentration, $\phi = \bar{\phi}$, and that particle conformation does not change along the streamlines, $\boldsymbol{u} \cdot \nabla \boldsymbol{M} = \boldsymbol{0}$.
2. **Symmetry line.** Because of symmetry, at the centerline of the channel we have that $\boldsymbol{n} \cdot \boldsymbol{u} = 0$, $\boldsymbol{t} \cdot (\boldsymbol{n} \cdot \boldsymbol{\Sigma}) = 0$ and $\boldsymbol{n} \cdot \boldsymbol{N}_\phi = 0$.
3. **Outflow plane.** We assumed a fully developed flow with fixed pressure and no diffusive flux of particles, $\boldsymbol{n} \cdot \nabla \boldsymbol{u} = \boldsymbol{0}$, $p = p_0$ and $\boldsymbol{n} \cdot \boldsymbol{N}_\phi = 0$.
4. **Channel walls.** We applied the no-slip and no-penetration conditions, which lead to $\boldsymbol{u} = \boldsymbol{0}$ and $\boldsymbol{n} \cdot \boldsymbol{N}_\phi = 0$.

Figure 2 summarizes the boundary conditions of the problem.

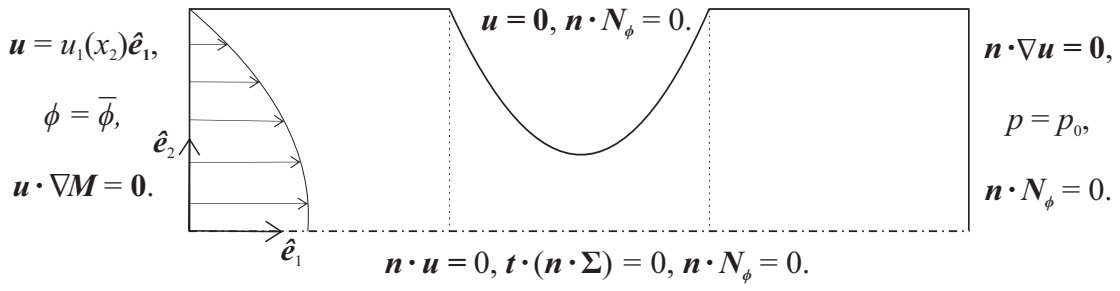

Figure 2: Boundary conditions for the flow through the converging-diverging channel.

3 SOLUTION METHOD

The transport equations governing the suspension flow are numerically solved using a slightly variation of the discrete elastic-viscous split stress, independent traceless velocity gradient interpolation, streamline upwind Petrov-Galerkin Finite Element Method (DEVSS-TG/SUPG FEM). This stable, robust numerical formulation was developed by Pasquali & Scriven (2002) and is based on the earlier works of Guénette & Fortin (1995) and Szady et al. (1995) on the flow of viscoelastic polymer solutions.

Particle transport and conformation equations deal with higher-order derivatives of the velocity field in their weighted residual formulations. However, these derivatives are discontinuous across the element boundaries, which leads to several numerical issues. In order to compute these terms, the DEVSS-TG formulation treat the velocity gradient as an additional independent variable of the problem with a continuous traceless interpolation, defined as

$$\boldsymbol{G} = \nabla \boldsymbol{u} - \frac{\nabla \cdot \boldsymbol{u}}{\boldsymbol{I} : \boldsymbol{I}} \boldsymbol{I}. \tag{11}$$

The variable $\boldsymbol{G}$ is called interpolated velocity gradient to distinguish it from the raw velocity gradient, $\nabla \boldsymbol{u}$. The use of a traceless interpolation for the velocity gradient is fundamental in the numerical computation of incompressible flows. In this case, Eq. (11) guarantees that $\text{tr}\, \boldsymbol{G} = 0$ regardless of the value of $\nabla \cdot \boldsymbol{u}$ calculated with the approximated velocity field, which may not be exactly divergence-free. The interpolated velocity gradient is used to rewrite the suspension stress tensor. Since there is no elastic stress in the flow, the viscous stress can be written as

$$\boldsymbol{\tau} = \eta(\phi)(\boldsymbol{G} + \boldsymbol{G}^T) + \eta_a(\nabla \boldsymbol{u} + \nabla \boldsymbol{u}^T - \boldsymbol{G} - \boldsymbol{G}^T), \tag{12}$$

where η_a is a numerical viscosity-like parameter, so that the second term on the right-hand side of Eq. (12) stabilizes the computational method. The introduction of this term is legitimate because this term is zero in the strong form of the equations and becomes vanishingly small in the weighted residual form as the approximate solution approaches the exact solution. All computations were made with a constant value of η_a. Changing the value of η_a has a little or no effect on the final numerical solution, provided that η_a is of the same order of magnitude of η_0.

Another numerical problem that may appear in the numerical computations of the problem is related to the singularity of the DFM in regions where the shear rate vanishes, as was reported by different researches considering the pressure-driven flows of suspensions through tubes and channels (Miller & Morris, 2006; Ahmed & Singh, 2011; Rebouças et al., 2016). In an effort to overcome this issue, we have used a modified version of the non-local stress contribution to the shear rate proposed by Miller & Morris (2006). Briefly, the procedure consists on define a non-local constant shear rate $\dot{\gamma}_\delta = \delta \dot{\gamma}_c$ to be added to the shear rate field to avoid the existence of regions of zero shear rate. Here, $\delta = 10^{-4}$ is a numerical parameter and $\dot{\gamma}_c = V/H$ is a characteristic shear rate of the flow. Note that the finite non-local contribution satisfies $\dot{\gamma}_\delta + \dot{\gamma} \approx \dot{\gamma}$ except in regions where $\dot{\gamma} \to 0$, giving the model the required effect of improving the numerical results near regions where the shear rate approaches zero.

Multiplying Eqs. (1), (2), (4) and (8) by weighting functions ψ_c, ψ_m, ψ_ϕ, ψ_M and ψ_G, integrating over the physical domain Ω (bounded by Γ) and applying the Gauss-Green-Ostrogradskii Theorem to the momentum and particle transport equations to lower the order of the highest derivatives of the independent variables yields the following weighted residual equations,

$$R^{c,\alpha} = \int_\Omega \psi_c^\alpha (\nabla \cdot \boldsymbol{u})\, d\Omega, \tag{13}$$

$$\boldsymbol{R}^{m,\alpha} = \int_\Omega \psi_m^\alpha \left[\rho\left(\frac{\partial \boldsymbol{u}}{\partial t} + \boldsymbol{u}\cdot\nabla\boldsymbol{u}\right)\right] d\Omega + \int_\Omega \nabla\psi_m^\alpha \cdot \boldsymbol{\Sigma}\, d\Omega - \int_\Gamma \boldsymbol{n}\cdot(\psi_m^\alpha \boldsymbol{\Sigma})\, d\Gamma, \tag{14}$$

$$R^{\phi,\alpha} = \int_\Omega \psi_\phi^\alpha \left(\frac{\partial \phi}{\partial t} + \boldsymbol{u}\cdot\nabla\phi\right) d\Omega - \int_\Omega \nabla\psi_\phi^\alpha \cdot \boldsymbol{N}_\phi\, d\Omega + \int_\Gamma \boldsymbol{n}\cdot(\psi_\phi^\alpha \boldsymbol{N}_\phi)\, d\Gamma, \tag{15}$$

$$\boldsymbol{R}^{M,\alpha} = \int_\Omega \psi_M^\alpha \left[\overset{\nabla}{\boldsymbol{M}} + 2\frac{\boldsymbol{D}:\boldsymbol{M}}{\boldsymbol{I}:\boldsymbol{M}}\boldsymbol{M} + \frac{1}{\lambda}(\boldsymbol{M}-\boldsymbol{I})\right] d\Omega, \tag{16}$$

$$\boldsymbol{R}^{G,\alpha} = \int_\Omega \psi_G^\alpha \left[\boldsymbol{G} - \nabla\boldsymbol{u} + \frac{\nabla\cdot\boldsymbol{u}}{\boldsymbol{I}:\boldsymbol{I}}\boldsymbol{I}\right] d\Omega. \tag{17}$$

In relation to Eqs. (13)-(17), the first superscript on the residual identifies the type of residual equation, and the second superscript labels the residual equation in the set. The independent variables of the problem are written as a linear combination of a finite number of basis functions, such that $p = p^\beta \varphi_p^\beta$, $\boldsymbol{u} = \boldsymbol{u}^\beta \varphi_u^\beta$, $\phi = \phi^\beta \varphi_\phi^\beta$, $\boldsymbol{M} = \boldsymbol{M}^\beta \varphi_M^\beta$ and $\boldsymbol{G} = \boldsymbol{G}^\beta \varphi_G^\beta$. Einstein's summation is assumed here. The subscript in the basis function denotes the variable that is approximated with that basis function, and is needed because different sets of basis function are used to approximate different variables. On the other hand, the superscript index in the basis functions identifies each basis function in the basis set and takes any value between one and the number of basis function in the set. Lagrangian biquadratic functions were used to represent the velocity field and the concentration field, Lagrangian bilinear functions for particle conformation and interpolated velocity gradient, and linear discontinuous functions for the pressure field. Galerkin's weighting functions were used in the residual equations of mass conservation, momentum conservation and interpolated velocity gradient, so that $\psi_c = \varphi_p$, $\psi_m = \varphi_u$ and $\psi_G = \varphi_G$. In turn, the stabilized Streamline-Upwind Petrov-Galerkin formulation was applied in both particle concentration and conformation equations, leading to $\psi_\phi = \varphi_\phi + h^u(\boldsymbol{u}\cdot\nabla\varphi_\phi)$ and $\psi_M = \varphi_M + h^u(\boldsymbol{u}\cdot\nabla\varphi_M)$, where h^u is the upwinding parameter, defined as the characteristic size of the smallest element in the computational mesh.

The domain was discretized using Q_2/P_{-1} quadrilateral finite elements, each one with 62 degrees of freedom. The DEVSS-TG/SUPG formulation leads to a large, sparse set of coupled, non-linear algebraic equations, which was solved using Newton's method with a numerical Jacobian matrix. The tolerance on the L2-norm of the global residual vector and Newton's update was set to 10^{-6}. At each iteration, the linear system was solved with a frontal solver based on the LU factorization method and solutions at different parameters were achieved with a first-order arclength continuation.

4 RESULTS

The spatial discretization was made with 1,200 finite elements and 4,961 nodes, and Fig. 3 shows the computational mesh used in the simulations. Stretching functions were used in order to concentrate elements near the contraction and channel walls. The resulting global system of non-linear algebraic equations has 28,731 degrees of freedom in this case.

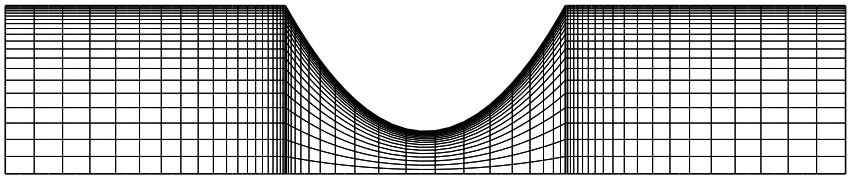

Figure 3: Representative mesh used in the simulations.

The results are given in a dimensionless way, where the unit of length in the $\hat{e}_1$-direction is the channel length, L, and in the $\hat{e}_2$-direction is half the channel height at the inflow plane, H. The imposed flow rate is expressed using the Reynolds number of the flow, which was defined as $Re = \rho V H/\bar{\eta}$, where ρ is the suspension density, V is the mean velocity of the flow and $\bar{\eta} = \eta(\bar{\phi})$ is the suspension viscosity evaluated with the bulk concentration (i.e. neglecting particle migration effects). The results for the average particle orientation are given in degrees. We have used suspensions of particles with $a = 1$ μm, $p = 2$ and $\tau = 1$ in a channel with $H = 100$ μm. In all simulations, $Re = 0.03$.

4.1 Particle concentration

Our first analysis is related to the effects of particle migration in the flow through the converging-diverging channel. In this sense, Fig. 4 shows the particle concentration profile along the channel centerline ($x_2 = 0$) for suspensions with different bulk concentrations.

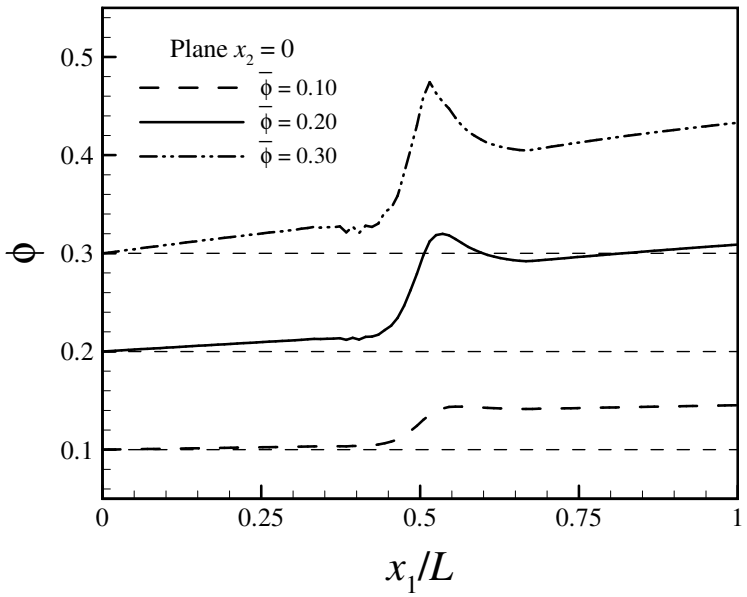

Figure 4: Particle concentration along the channel centerline varying the suspension bulk concentration.

From Fig. 4, one views that the particle concentration along the channel centerline is always equal or higher than the suspension bulk concentration (denoted by the dashed horizontal lines), ensuring that the particles migrate from the wall, where the shear rate is maximum, to the center of the channel, where the shear rate approaches zero. This result is in good agreement with the predictions of the DFM. Note, however, that the rate of increasing of particle concentration along the centerline depends on the position along the channel. Indeed, for a given bulk concentration, the particle concentration increases with approximately the same rate upstream and downstream the contraction. On the other hand, the presence of the contraction at the middle of channel increases the flux of particles from the wall towards the centerline, so that the maximum concentration always occurs near the contraction. For instance, the maximum value predicted for particle concentration is $\phi \approx 0.47$ for $\bar{\phi} = 0.30$, $\phi \approx 0.32$ for $\bar{\phi} = 0.20$, and $\phi \approx 0.14$ for $\bar{\phi} = 0.10$, and occur at $x_1/L \approx 0.51$ in all cases. The driving force for particle migration is the spatial variation of interparticle collisions related to gradients in shear rate due to the non-homogeneous shear flow, and a simple analysis of the flow kinematics can explain these results. In order to satisfy the mass conservation principle, the flow accelerates at the entrance of the contraction, increasing the shear rate and its gradients, and thereby increasing the flux of particles towards the center of channel. In turn, the mean velocity of the flow is the same upstream and downstream the contraction, leading to approximately the same particle flux from the wall to the centerline.

The predictions of particle concentration at the contraction ($x_1/L = 0.5$) and at the outflow plane ($x_1/L = 1$) for the same cases are presented in Fig. 5. These results confirm, again, the migration of particles from the wall to the channel centerline. Draws attention that, for a given bulk concentration, the shape of the profiles of particle concentration at the contraction and at the outflow are almost the same, with slightly differences at the wall and centerline. However, the total amount of particles at these sections are considerably different in order to conserve the total convective flux of particles in the flow, which is defined as $\int_S \boldsymbol{u}(\boldsymbol{x})\phi(\boldsymbol{x}) \cdot \boldsymbol{n}\, dS$. In other words, this integral quantity is constant, so that, as the velocity increases, the local concentration of particles decreases.

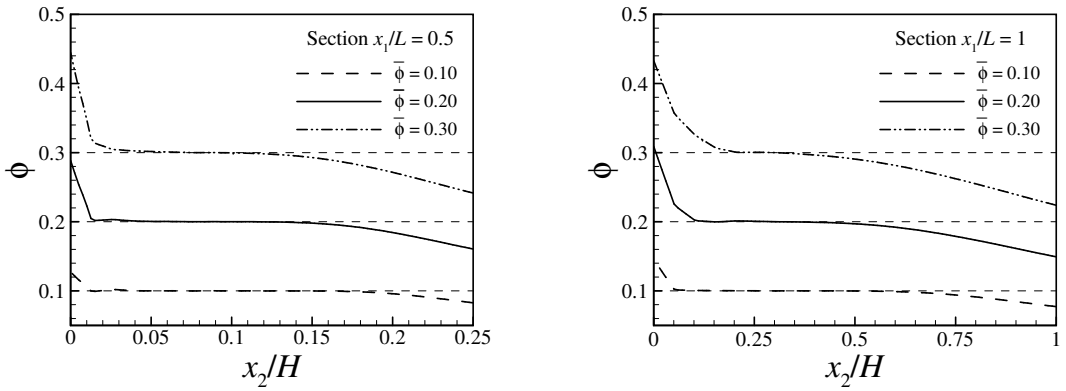

Figure 5: Particle concentration in the channel varying the suspension bulk concentration. In (a), at the contraction ($x_1/L = 0.5$); in (b), at the outflow plane ($x_1/L = 1$).

Figure 6 summarizes these results and shows a color map of particle distribution in the domain for the case in which $\bar{\phi} = 0.30$, highlighting the effect of the contraction in increasing the flux of particles from the wall to the centerline of the channel.

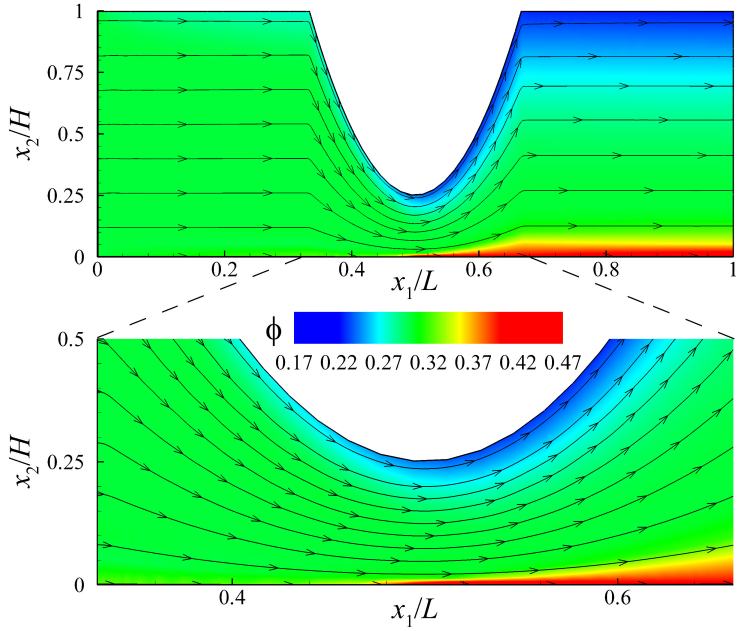

Figure 6: Color map of particle concentration in the converging-diverging channel, highlighting the local concentration of particles in the contraction. Predictions at $\bar{\phi} = 0.30$.

4.2 Particle alignment

Now, let us consider the particle alignment in the converging-diverging channel, investigating the average particle orientation in shear-dominated and extensional-dominated regions in the flow domain. Figure 7 shows the average particle orientation along the channel symmetry line ($x_2 = 0$) varying the suspension bulk concentration. The particles experience a very strong variation in their alignment as the suspensions flows through the channel. Upstream the contraction, where the flow is dominated by shear, the orientation of the particles remains almost constant and equal to $\theta \approx 63°$, regardless of the value of $\bar{\phi}$. As the contraction approaches, the flow accelerates, so that uniaxial extensional effects are predominant. Hence, the particles tend to align with respect to the flow direction and there is a great decrease in the value of θ near the contraction entrance. The minimum value predicted occurs at $x_1/L \approx 0.37$ and is $\theta \approx 3.5°$ for all cases considered. Otherwise, at the end of the contraction, the flow decelerates, so that biaxial extensional effects are predominant, and the particles tend to align perpendicular to the flow direction. For instance, the maximum value predicted for θ occurs at $x_1/L \approx 0.67$, and is $\theta \approx 84°$ for $\bar{\phi} = 0.10$, $\theta \approx 84.5°$ for $\bar{\phi} = 0.20$ and $\theta \approx 87.5°$ for $\bar{\phi} = 0.30$. Then, the angle θ decreases from its maximum to a lower value, which remains almost constant at the downstream region, where the flow is once again dominated by shear effects. The three profiles are virtually the same from the inflow plane to $x_1/L \approx 0.57$. In turn, downstream the contraction we have that the particle alignment depends on the suspension concentration, varying from $\theta \approx 61.4°$ for $\bar{\phi} = 0.10$ to $\theta \approx 74.5°$ for $\bar{\phi} = 0.30$ at the outflow plane.

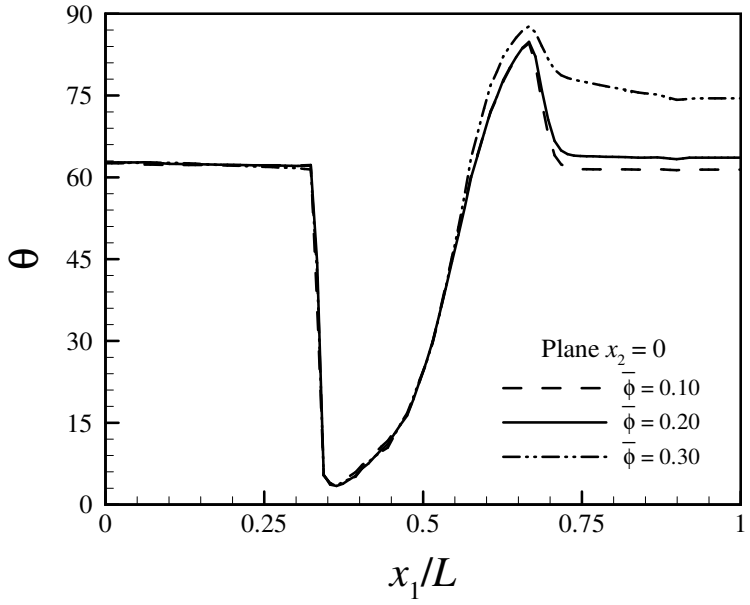

Figure 7: Average particle orientation along the channel centerline varying the suspension bulk concentration.

Figure 8 presents the profiles for particle orientation just before and just after the contraction ($x_1/L = 1/3$ and $x_1/L = 2/3$, respectively), and these results confirm the analysis discussed so far. One observes that the particles orientation varies from $\theta \approx 42^\circ$ to $\theta \approx 85^\circ$ along the symmetry line from the section just before the contraction to the section just after the contraction, regardless of the value of $\bar{\phi}$. In both sections the particle alignment near the wall is very similar, being $\theta \approx 25^\circ$ for all cases considered.

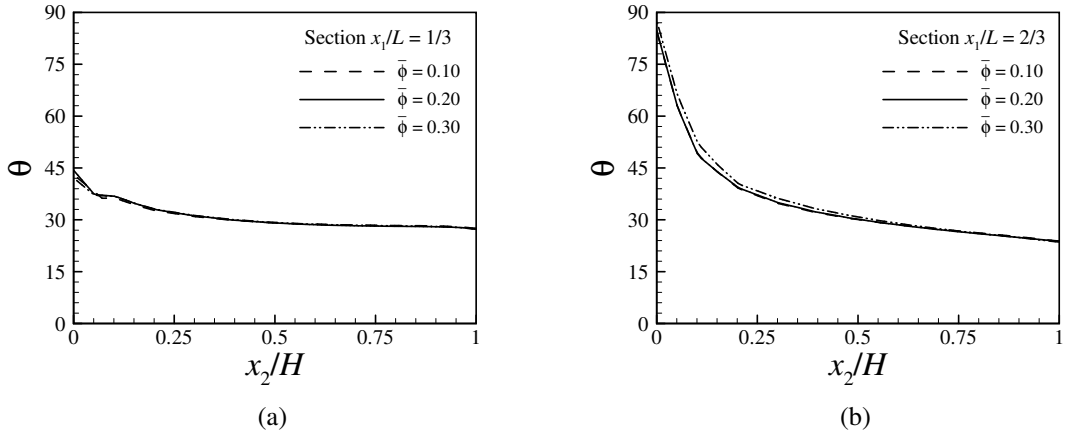

(a) (b)

Figure 8: Average particle orientation in the channel varying the suspension bulk concentration. In (a), just before the contraction ($x_1/L = 1/3$); in (b), just after the contraction ($x_1/L = 2/3$).

The results of Figs. 7 and 8 show that the particle alignment strongly depends on the flow kinematics, which forces the particles to orient in the stretching direction. As a matter of fact, the orientation of the particles remain almost constant in regions dominated by shear. On the other hand, in regions where the flow is convergent and dominated by uniaxial extensions, the particles tend to align with respect to the flow direction ($\theta \to 0°$), and in regions where the flow is divergent and dominated by biaxial extensions, the particles align perpendicular to the flow direction ($\theta \to 90°$). Figure 9 illustrates a color map of average particle orientation in the flow for $\bar{\phi} = 0.30$, and summarizes the results discussed so far.

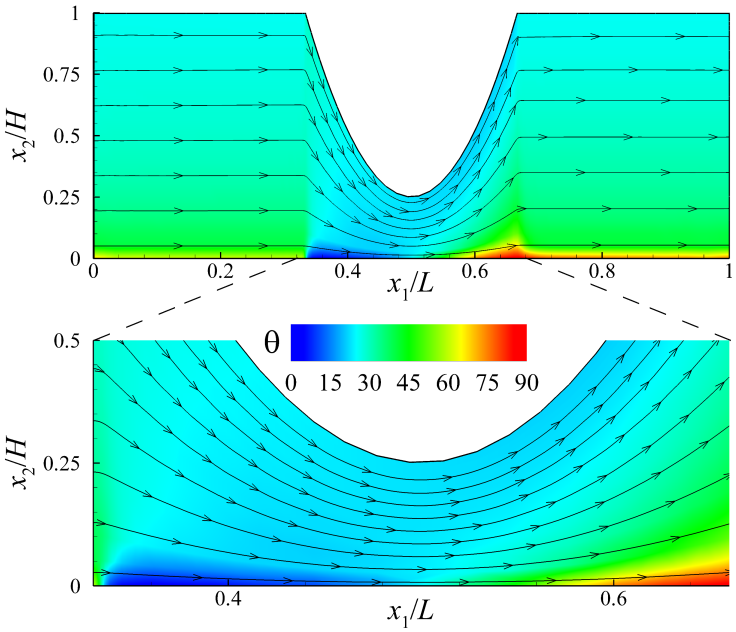

Figure 9: Color map of average particle orientation in the converging-diverging channel, highlighting the local orientation of particles in the contraction. Predictions at $\bar{\phi} = 0.30$.

It is remarkable that our numerical predictions agree very well with some experimental results recently available in the literature of suspensions flows. For instance, the experiments of Trebbin et al. (2013) have showed that anisotropic cylindrical micelles align parallel to the flow direction at the entrance of the contraction, and perpendicular to the flow direction at the end of the contraction in the flow through a converging-diverging tube. The same qualitative results were obtained by Oumer & Mamat (2013) with suspensions of long fibers in reinforced polymer composites.

5 FINAL REMARKS

This work studied particle migration and particle alignment phenomena in the flow of suspensions of elliptical particles. We considered the flow through a converging-diverging channel to investigate particle dynamics in shear-dominated and extensional-dominated regions. The model considers two additional equations accounting for particle migration and particle orientation in the flow. Particle migration was modeled according to the Diffusive Flux Model

developed by Phillips et al. (1992) with an additional curvature-induced flux (Kim et al., 2008), whereas the average particle orientation was evaluated using the principal direction of a particle conformation tensor. The transport of conformation in the flow was obtained from the model proposed by Pasquali & Scriven (2002, 2004), and the constitutive relation to define the suspension stress tensor was adapted from models used to describe the flow of suspensions of spheroids, cylinders and long fibers (Larson, 1988, 1999). The resulting fully coupled, non-linear model was solved using a slightly variation of the DEVSS/TG-SUPG Finite Element Method, and several aspects of the numerical methodology employed were discussed, such as the use of a traceless velocity gradient interpolation, an adaptive viscous stress, and a non-local shear stress to overcome the singularity of the DFM.

The results show that the particles tend to migrate against gradients in shear rate, moving from the wall, where the shear rate is maximum, to the channel centerline, where the shear rate approaches zero. These predictions are in very good agreement with the DFM. Because of the contraction in the middle of the channel, the fluid accelerates and increases the gradients in shear rate in this region. As a consequence, the contraction increases the diffusive flux of particles towards the center of the channel. In all cases, we found that the maximum local concentration of particles occurred inside the contraction zone. In addition, the average particle orientation strongly depends on the flow kinematics. The alignment of the particles remains almost constant in shear-dominated regions, as occurs upstream and downstream the contraction. On the other hand, the particles tend to align to the flow direction in converging flows dominated by uniaxial extensions, as occurs at the entrance of the contraction, and perpendicular to the flow direction in diverging flows dominated by biaxial extensions, as occurs at the end of the contraction. Our model recovers very well the experimental results of Trebbin et al. (2013) and Oumer & Mamat (2013) on the alignment of long fibers suspensions in converging-diverging tubes.

ACKNOWLEDGEMENTS

The authors would like to acknowledge the financial support from the Brazilian Research Council (CNPq) and the Industrial Partnership for Research in Interfacial Materials & Engineering (IPrime - University of Minnesota).

REFERENCES

Abbott, J. R., Tetlow, N., Graham, A. L., Altobelli, S. A., Fukushima, E., Mondy, L. A., & Stephens, T. S., 1991. Experimental observations of particle migration in concentrated sus pensions: Couette flow. *Journal of Rheology*, vol. 35, pp. 773-797.

Ahmed, G. M. Y. & Singh, A., 2011. Numerical simulation of particle migration in asymmetric bifurcation channel. *Journal of Non-Newtonian Fluid Mechanics*, vol. 166, pp. 42-51.

Altobelli, S. A. & Givler, R. C., 1991. Velocity and concentration measurements of suspensions by nuclear magnetic resonance imaging. *Journal of Rheology*, vol. 35, 721-734.

Bicerano, J., Douglas, J. F., & Brune, D. A., 1999. Model for the viscosity of particle dispersions. *Journal of Macromolecular Science C*, vol. 39, pp. 561-642.

Brady, J. F., 1993. The rheological behavior of concentrated colloidal dispersions. *Journal of Chemical Physics*, vol. 99, pp. 567-581.

Chow, A. W., Sinton, S. W., Iwamiya, J. H., & Stephens, T. S., 1994. Shear-induced migration in Couette and parallel-plate viscometers: NMR imaging and stress measurements. *Physics of Fluids*, vol. 6, pp. 2561-2576.

Donev, A., Connelly, R., Stillinger, F. H., & Torquato, S., 2007. Under constrained jammed packings of non-spherical hard particles: Ellipses and ellipsoids. *Physical Review E*, vol. 75, pp. 051304 1-32.

Donev, A., Sachs, I. C. D., Variano, E. A., Stillinger, F. H., & Connelly, R., 2004. Improving the density of jammed disordered packings using ellipsoids. *Science*, vol. 303, pp. 990-993.

Einstein, A., 1911. Berichtigung zu meiner arbeit: Eine nene bestimmung der molekuldimension. *Annalen der Physik*, vol. 34, pp. 591-592.

Gadala-Maria, F. & Acrivos, A., 1980. Shear-induced structure in a concentrated suspension of solid spheres. *Journal of Rheology*, vol. 24, pp. 799-814.

Graham, A. L. & Altobelli, S.A, 1991. NMR imaging of shear-induced diffusion and structure in concentrated suspensions. *Journal of Rheology*, vol. 35, pp. 191-201.

Guénette, R. & Fortin, M., 1995. A new mixed finite element method for computing viscoelastic flows. *Journal of Non-Newtonian Fluid Mechanics*, vol. 60, pp. 27-52.

Hampton, R. E., Mammoli, A. A., Graham, A. L., Tetlow, N., & Altobelli, S. A., 1997. Migration of particles undergoing pressure-driven flow in a circular conduit. *Journal of Rheology*, vol. 41, pp. 621-640.

Han, M., Kim, C., Kim, M., & Lee, S., 1999. Particle migration in tube flow of suspensions. *Journal of Rheology*, vol. 43, pp. 1157-1174.

Jeffery, G. B., 1922. The motion of ellipsoidal particles immersed in a viscous fluid. *Proceedings of the Royal Society of London A*, vol. 102, pp. 161-179.

Karnis, A., Goldsmith, A. L., & Mason, S. G., 1966. The kinetics of flowing dispersions: Concentrated suspensions of rigid particles. *Journal of Colloid and Interface Science*, vol. 22, pp. 531-553.

Kim, J. M., Lee, S. G., & Kim, C., 2008. Numerical simulations of particle migration in suspension flows: Frame-invariant formulation of curvature-induced migration. *Journal of Non-Newtonian Fluid Mechanics*, vol. 150, pp. 162-176.

Kistler, S. F. & Schweizer, P. M., 1997. *Liquid film coating*. Chapman & Hall.

Koh, C. J., Hookham, P., & Leal, L. G., 1994. An experimental investigation of concentrated suspension flows in a rectangular channel. *Journal of Fluid Mechanics*, vol. 266, pp. 1-32.

Krieger, I. M., 1972. Rheology of monodisperse latices. *Advances in Colloid and Interface Science*, vol. 3, pp. 111-136.

Krieger, I. M. & Dougherty, T. J., 1959. A mechanism for non-Newtonian flow in suspensions of rigid spheres. *Transactions of The Society of Rheology*, vol. 3, pp. 137-152.

Kulshreshtha, A. K., Singh, O. N., & Wall, G. M., 2010. *Pharmaceutical Suspensions: From Formulation Development to Manufacturing*. Springer.

Landau, L. D., Lifshitz, E. M., & Pitaevskii, L. P., 1984. *Electrodynamics of Continuous Media*.

Pergamon Press.

Larson, R. G., 1988. *Constitutive equations for polymer melts and solutions*. Butterworths Books.

Larson, R. G., 1999. *The Structure and Rheology of Complex Fluids*. Oxford University Press.

Leighton, D. & Acrivos, A., 1987. The shear-induced migration of particles in concentrated suspensions. *Journal of Fluid Mechanics*, vol. 181, pp. 415-439.

Lyon, M. K. & Leal, L. G., 1998. An experimental study of the motion of concentrated suspensions in two-dimensional channel flow Part 1 : Monodisperse systems. *Journal of Fluid Mechanics*, vol. 363, pp. 25-56.

Miller, R. M. & Morris, J. F., 2006. Normal stress-driven migration and axial development in pressure-driven flow of concentrated suspensions. *Journal of Non-Newtonian Fluid Mechanics*, vol. 135, pp. 149-165.

Oumer, A. N. & Mamat, O., 2013. A review of effects of molding methods, mold thickness and other processing parameters on fiber orientation in polymer composites. *Asian Journal of Scientific Research*, vol. 6, pp. 401-410.

Pasquali, M. & Scriven, L. E., 2002. Free surface flows of polymer solutions with models based on the conformation tensor. *Journal of Non-Newtonian Fluid Mechanics*, vol. 108, pp. 363-409.

Pasquali, M. & Scriven, L. E., 2004. Theoretical modeling of microstructured liquids: a simple thermodynamic approach. *Journal of Non-Newtonian Fluid Mechanics*, vol. 120, pp. 101-135.

Phillips, R. J., Armstrong, R. C., Brown, R. C., Graham, A. L., & Abbott, J. R., 1992. A constitutive equation for concentrated suspensions that accounts for shear-induced particle migrations. *Physics of Fluids*, vol. 4, pp. 30-40.

Rebouças, R. B., Siqueira, I. R., de Souza Mendes, P. R., & Carvalho, M. S., 2016. On the pressure-driven flow of suspensions: particle migration in shear sensitive liquids. *Journal of Non-Newtonian Fluid Mechanics*, vol. 234, pp. 178–187.

Santamaría-Holek, I. & Mendoza, C. I., 2009. The rheology of hard sphere suspensions at arbitrary volume fractions: an improved differential viscosity model. *Journal of Chemical Physics*, vol. 130, pp. 044904 1-7.

Santamaría-Holek, I. & Mendoza, C. I., 2010. The rheology of concentrated suspensions of arbitrarily-shaped particles. *Journal of Colloid and Interface Science*, vol. 346, pp. 118-126.

Schramm, L. L., 1996. *Suspensions: Fundamentals And Applications In The Petroleum Industry*. American Chemical Society.

Shewan, H. M. & Stokes, J. R., 2015. Analytically predicting the viscosity of hard sphere suspensions from the particle size distribution. *Journal of Non-Newtonian Fluid Mechanics*, vol. 222, pp. 72-81.

Sinton, S. A. & Chow, A., 1991. NMR flow imaging of fluids and solid suspensions in Poiseuille flow. *Journal of Rheology*, vol. 35, pp. 735-772.

Subia, S. R., Ingber, M. S., Mondy, L. A., Altobelli, S. A., & Graham, A. L., 1998. Modelling of concentrated suspensions using a continuum constitutive equation. *Journal of Fluid Mechanics*,

vol. 373, pp. 193-219.

Szady, M. J., Salamon, T. R., Liu, A. W., Armstrong, R. C., & Brown, R. A., 1995. A new mixed finite element method for viscoelastic flows governed by differential constitutive equations. *Journal of Non-Newtonian Fluid Mechanics*, vol. 59, pp. 215-243.

Trados, T. F., 2011. *Rheology of Dispersions: Principles and Applications*. John Wiley & Sons.

Trados, T. F., 2012. *Dispersion of Powders in Liquids and Stabilization of Suspensions*. John Wiley & Sons.

Trebbin, M., Steinhauser, D., Perlich, J., Buffet, A., Roth, S. V., Zimmermann, W., Thiele, J., & Frster, S., 2013. Anisotropic particles align perpendicular to the flow direction in narrow microchannels. *Proceedings of the National Academy of Sciences*, vol. 110, pp. 6706-6711.